AnyScatter: Eliminating Technology Dependency in Ambient Backscatter Systems

Taekyung Kim and Wonjun Lee
Network and Security Research Lab.
School of Information Security
Korea University, Seoul, Republic of Korea
{tkkim92, wlee}@korea.ac.kr

***Abstract*—In this paper, we introduce technology-independent ambient backscatter systems where a backscatter tag utilizes all single-stream ambient signals transmitted by nearby devices. Specifically, we design a phase demodulation algorithm that detects a backscatter signal from the phase difference between the two antennas, no matter which signal the tag reflects. We then develop a parallelized backscatter receiver that mitigates the dead spot problem by leveraging antenna diversity. To show the feasibility of our design, we implement a backscatter receiver on the software-defined radio platform and analyze 50 MHz RF bandwidth in real-time. Our evaluation shows that the receiver can decode backscatter bits carried by any single stream ambient signal such as a continuous wave, a QAM signal, and even a noise signal. We also demonstrate backscatter transmissions with commodity Wi-Fi and Bluetooth devices to prove that our design can be combined with existing wireless networks.**

***Index Terms*—Ambient backscatter, Internet of Things, Low-power Wireless Networks**

I. Introduction

Backscatter is a key enabler for long-term deployment of energy-constrained wireless devices such as energy harvesting sensors. Unlike conventional wireless devices, a backscatter tag does not generate wireless signals. Instead, the tag modulates data bits on to a carrier signal transmitted from a dedicated device by changing its load impedance. The simple circuitry of this mechanism consumes almost zero energy for data transmission. Furthermore, in recent years, researchers have improved the energy efficiency of sensor devices by tightly integrating a backscatter module with data handling and sensing components [1]–[3]. It is obvious that backscatter brings several advantages for ultra-low power systems, but the deployment of carrier sources is a prerequisite.

As an answer to the problem, several ambient backscatter systems have been proposed in the past few years. The key idea of ambient backscatter is to replace dedicated carrier sources with pre-deployed wireless devices. Initially, researchers have implemented a hardware prototype to demonstrate tag-to-tag backscatter communications over ambient TV tower signals [4, 5]. And then these efforts are extended to tag-to-gateway schemes, because tags eventually have to be connected to the Internet through some devices. From this perspective, the computational power of the backscatter receiver is improved than in the tag-to-tag system model. These changes induce the ambient backscatter system to utilize a wider variety of carrier signals.

Wi-Fi backscatter is one of the well-known examples of tag-to-gateway ambient backscatter systems [6]–[8]. The tag operates the same way as passive RFID tags, whereas the receiver performs Wi-Fi frame decoding as well as backscatter signal detection from soft errors in received Wi-Fi symbols. Another approach to establishing a backscatter link over ambient signals is side-band backscatter. If the clock rate of the tag is faster than the bandwidth of the ambient transmitter, the tag can create a copy of a received signal on the side band. Based on this technique, researchers have successfully demonstrated backscatter transmission based on Wi-Fi, Bluetooth, LoRa and FM radio signals in recent years [9]–[13]. However, these efforts are designed for a specific wireless technology, thus only a small portion of ambient signals can be used for backscatter transmissions while other signals are treated as interference.

With this point in view, we introduce AnyScatter, a technology-independent ambient backscatter system that utilizes all nearby single-stream wireless devices for backscatter transmission. The starting point of this approach is the difference in received phase at each antenna due to the time difference of arrival for each wireless propagation path. Since the wireless propagation paths from the transmitter to the receiver are consistent within one frame duration in indoor environments, the phase difference is also consistent regardless of what signal is transmitted. However, this claim is not true for backscatter systems. A tag creates an additional wireless propagation path by reflecting incident signals. If the tag changes its reflection coefficient, the channel of the reflected path also changes. We focus on this aspect to design a technology-independent ambient backscatter receiver. The receiver keeps monitoring the phase difference for backscatter signal detection. When a tag reflects an ambient signal, the phase difference shows the transition between the two states according to the reflection coefficient of the tag. The sequence of the state transitions refers to the data bits transmitted from the tag.

We then scale out our approach in parallel. Similar to the phase cancellation problem in envelope detector-based schemes [14], the receiver cannot observe a backscatter signal in some wireless channel conditions. Our solution to this problem is diversifying wireless channels at the receiver. Based on the expectation that there is at least one antenna pair that

is not in the dead spot, we increase the number of antennas at the receiver and parallelize backscatter demodulation procedures. The receiver analyzes the phase differences for all combinations of antenna pairs in parallel and then ignores the duplicated backscatter frames decoded simultaneously on different pairs of antennas. Next, we append envelope detector-based schemes to our receiver design. Even though these schemes can only be used for constant magnitude ambient signals, the receiver can benefit from parallelization for those signals.

In this paper, we investigate if it is possible to eliminate technology dependency in ambient backscatter systems. In response to this question, our novel approach, AnyScatter, makes three contributions as follows:

- We propose a technology-independent backscatter receiver that decodes a backscatter frame from all types of single-stream ambient signals.
- We address the dead spot problem by designing a parallelized backscatter receiver that utilizes wireless channel diversity provided by multiple antennas.
- We develop an AnyScatter system on the software-defined radio platform and conduct extensive experiments to demonstrate backscatter transmissions over several types of ambient signals.

The rest of this paper is organized as follows. Section II gives the design preliminary on ambient backscatter systems. Section III introduces how we eliminate technology dependency in ambient backscatter systems. We validate and evaluate our approach in Section IV. We review the related work in Section V. Finally, Section VI concludes this paper.

II. System Model

Our system model is shown in Fig. 1. All wireless devices transmitting a single-stream signal are used as carrier sources. The tag reflects incident signals to represent data bits in the same way as passive RFID tags. The two different reflection coefficients of the tag correspond to bits '0' and '1'. The direct path signal from the ambient source and the reflected signal passing through the tag arrive at the receiver. The receiver separates the two signals and infers the state of the tag from the reflected signal. In the case of RFID systems, the effect of the tag is evident because a carrier source emits a continuous sinusoidal signal. The changes in the received signal are solely affected by the tag. However, a carrier signal is not constant in ambient backscatter systems. The receiver has to distinguish between the effect of the ambient source and the effect of the tag. Recent ambient backscatter systems have addressed this challenge by selecting a specific type of a carrier source, such as FM radio or Wi-Fi. By contrast, we tackle this challenge directly without wireless technology constraints. In this paper, we omit source-to-tag transmission to focus our discussion on backscatter transmission. There are novel techniques, such as Glaze [15], AM emulation [10] and packet length modulation [16], that can be integrated with our design. We leave this implementation as future work.

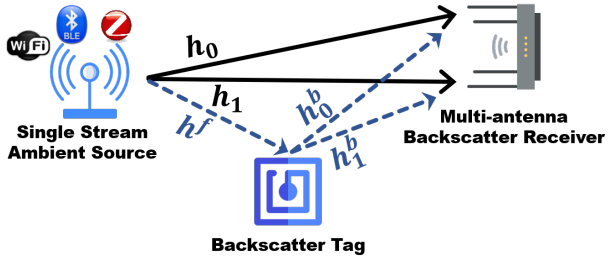

Fig. 1. High level illustration of AnyScatter system model

Before going to details, we construct a model of received signals at a multi-antenna receiver. Our design is based on digital communication systems where a wireless signal is represented as a sequence of complex numbers. In this context, we represent a transmitted signal from an ambient source as $x[n]$. We do not consider how the ambient signal is modulated and which data bits the signal is carrying. The bandwidth and the carrier frequency are also out of our interest. The only requirement is that the transmitted signal is in the receiver's frequency range. The receiver samples the signal with the period T. Under the assumption that antenna spacing is less than a few tens of centimeters as conventional multi-antenna receivers, each antenna of the receiver gets the sample $x[n]$ at the same time. For a 100 MHz sampling rate receiver, a wireless signal propagates 3 m ($= \frac{3 \cdot 10^8}{100 MHz}$) between the sampling period. Hence, an ambient signal received at the antenna i is given by:

$$s_i[n] = (h_i * x)[n] = \sum_{\tau=0}^{L-1} h_i[\tau] x[n-\tau] \tag{1}$$

where h_i is the channel impulse response from the ambient source to the receiver antenna i and L is the channel length.

Next, we construct a model of a backscatter signal. In this paper, we consider a binary phase-shift keying backscatter tag. The phase shift of the reflected signal is 0 and π. Each state corresponds to bits '0' and '1'. From the viewpoint of the receiver, the backscatter signal is a part of multipath propagation. The difference compared to normal propagation paths is that the wireless channel of the path changes. The backscatter signal received by the antenna i can be formulated as follows.

$$b_i[n] = (((h^f * x)[n] \cdot t[n]) * h_i^b)[n] \tag{2}$$

where h^f is the source-to-tag forward channel impulse response, h_i^b is the tag-to-receiver backward channel impulse response for an antenna i, and $t[n]$ is the phase shift of the tag. We approximate this signal as $b_i[n] = (\hat{h}_i * x)[n] t[n]$ by applying the associative property of convolution. We combine the forward and backward channel into a single channel $\hat{h}_i[n] = (h_{i,f} * h_{i,b})[n]$. And then, we approximate $t[n]$ as a scalar value, because the length of the combined channel impulse response $\hat{h}_i$ is much smaller than a backscatter symbol duration, which is at least a few μs in our system model. As

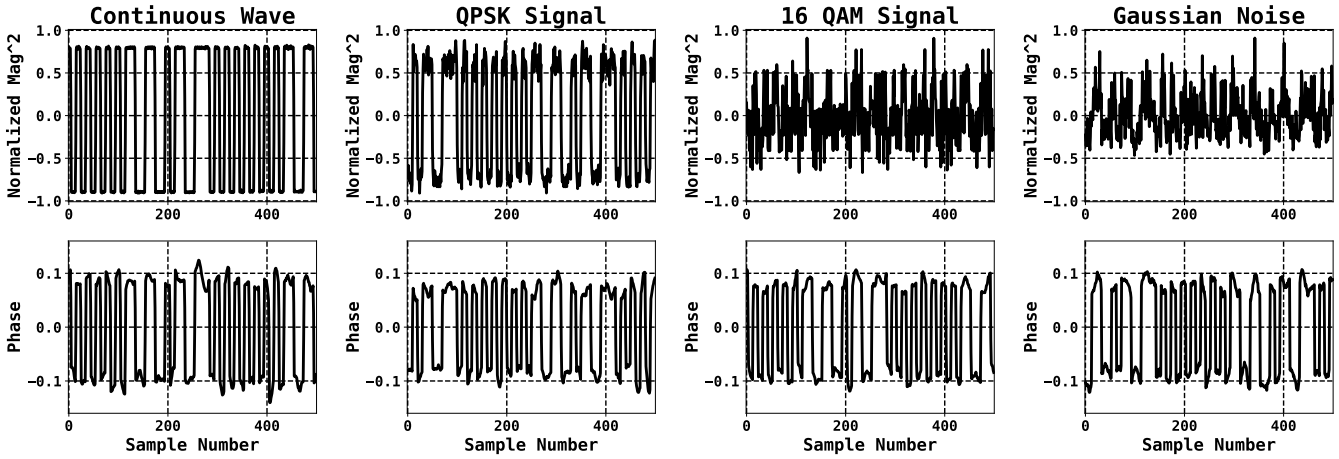

Fig. 2. Magnitude and phase difference of received signals for different types of ambient sources.

a result of approximation, the receiver observes the following signal at the antenna i.

$$r_i[n] = s_i[n] + b_i[n] = \begin{cases} ((h_i + \hat{h}_i) * x)[n] & \text{if } t[n] = e^{j\cdot 0} \\ ((h_i - \hat{h}_i) * x)[n] & \text{if } t[n] = e^{j\cdot \pi} \end{cases} \quad (3)$$

This equation describes how the backscatter signal is inserted to single-stream ambient signals. The radio characteristics of the ambient source, such as a modulation scheme and a center frequency, are abstracted to $x[n]$ in this equation without loss of generality. However, since the radio characteristics of the receiver and ambient sources are different in most cases, $x[n]$ should be considered as a random complex number when we design a backscatter receiver, in contrast to other ambient backscatter systems that have exploited technology-dependent patterns inside $x[n]$.

III. AnyScatter Design

In this section, we elaborate on the AnyScatter design. We first design a phase demodulation algorithm that eliminates technology dependency of ambient backscatter systems. We then mitigate the dead spot problem by scaling-out our design in parallel.

A. Phase Demodulation Algorithm

The rationale behind our approach is that the phase difference of each antenna is coherent within one frame duration, no matter which radio the ambient source uses. We extend this observation to ambient backscatter signal detection. The phase difference is a function of wireless propagation paths. If the wireless channels are coherent, the phase difference remains at a constant value. In the same way, when the tag switches its reflection coefficient, the receiver observes another phase difference value due to the change at the wireless propagation path passing through the tag. To prove that our approach is viable and independent to wireless technologies, we analyze the conjugate multiplication of received signals from two different antennas.

$$\begin{aligned} r_1[n]r_2^*[n] &= (s_1[n] + b_1[n])(s_2[n] + b_2[n])^* \\ &\approx s_1[n]s_2^*[n] + s_1[n]b_2^*[n] + b_1[n]s_2^*[n] \end{aligned} \quad (4)$$

In this equation, $\angle r_1[n]r_2^*[n]$ denotes the phase difference of the two signals. For simplicity, we omit the conjugate multiplication of two backscatter signals $b_1[n]b_2^*[n]$, which is negligible compared to other terms. Next, we analyze the expected value of the first term.

$$E[s_1[n]s_2^*[n]] = \sum_{\tau}\sum_{\delta} h_1[\tau]h_2^*[\delta]E[x[n-\tau]x^*[n-\delta]] \quad (5)$$

The inner part of the summation consists of the two components, the effect of wireless channels $h_1[\tau]h_2^*[\delta]$ and the effect of a ambient signal $E[x[n-\tau]x^*[n-\delta]]$. The latter component can be divided into two cases. In the case of $\tau \neq \delta$, the result converges to zero because it is equal to the summation of zero-mean random complex numbers. In the case of $\tau = \delta$, the result is the average signal strength of the ambient source $P_x = E[\|x[n]\|]$. Therefore, what we should care about is the second case, so the expected value becomes $P_x \sum_\tau h_1[\tau]h_2^*[\tau]$. The second and third terms of Eq. (4) can be derived in the same way. After taking the conjugate multiplication, the effect of the ambient source is converted to the average signal strength P_x. This can be regarded as a constant value within the corresponding frame duration, because the moving average window size of the receiver is much longer than the symbol duration and data bits are evenly distributed in most cases. In summary, the expected value of the conjugate multiplication for two received signals is the sum of the channel impulse responses for each propagation path scaled by the transmitter power.

To validate our claim, we conduct a pilot experiment with a USRP N210 and a USRP X310 for a source and a receiver respectively. The source transmits four types of carrier signals, a continuous wave, a QPSK signal, a 16 QAM signal, and

a noise signal. We place a BPSK tag next to the ambient source. The receiver monitors the phase difference between the two antennas and the magnitude of the received signal. The magnitude is the same as the output of an envelope detector, which is widely used in passive radio and tag-to-tag backscatter systems [14, 17]. Fig. 2 shows the magnitude and the phase difference for each carrier signal. For a continuous wave and a QPSK signal, the state transitions of the tag are clearly observed from both the magnitude and the phase difference. However, in the cases of a 16 QAM signal and a noise signal, we cannot observe the state transitions from the magnitude. The two carrier signals do not remain at a fixed magnitude anymore, so the received magnitude is affected by the tag as well as the carrier signals. By contrast, the phase difference shows the two distinct states for all types of carrier signals, because the effects of carrier signals are converted to a constant value as we derived in Eq. (5). This experiment shows that our approach successfully cancels the effects of ambient signals and that the phase difference can be used for backscatter demodulation.

The phase demodulation algorithm consists of the following steps. Assume that a receiver of a sample rate N demodulates a backscatter signal of a data rate M. $r_1[n]$ and $r_2[n]$ are the received samples from the two different antennas. First, the receiver calculates $r_1[n]r_2^*[n]$ for every received sample. And then, the output is decimated to the tag rate M. We take the average for every N/M samples with the early-late gate synchronizer in this stage [18]. The phase of the decimated sample shows the two clusters as shown in Fig. 2. To convert the sequence of the phase values into backscatter bits, the receiver keeps updating temporary variables C_0 and C_1 for every decimated sample. The receiver outputs a bit '0' and sets C_0 to $r_1[n]r_2^*[n]$ if $|\angle C_0^* r_1[n]r_2^*[n]| < |\angle C_1^* r_1[n]r_2^*[n]|$, and vice versa. When the receiver produces K consecutive bits, the receiver concludes that there was a sudden change in ambient signals and sets C_0 and C_1 to $r_1[n]r_2^*[n]$ and $r_1[n-1]r_2^*[n-1]$ as an initialization procedure.

Like other conventional backscatter systems such as RFID, our design assume that a backscatter frame contains a preamble and a cyclic redundancy check (CRC) field. C_0 and C_1 are used to distinguish two different phase clusters, thus we cannot sure whether the two variables represent the correct bits. For this reason, the receiver compares the received bits with the preamble as well as the flipped preamble. This comparison is for frame detection and temporary variable swapping as needed. On the other hand, the probability that noise samples pass this comparison test for a preamble of length l bits is $\frac{1}{2^{l-1}}$. Hence, the CRC has to be appended at the end of the frame so as not to return a frame made by noise samples and to ensure data integrity.

B. Parallelized Backscatter Receiver

Similar to the phase cancellation problem of the envelope detection receiver [14], the phase difference cannot describe a backscatter signal in some wireless channel conditions. Fig. 3 shows the example of the dead spot problem in our approach.

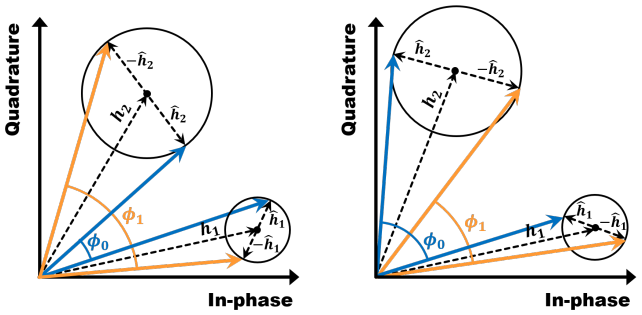

(a) Detectable channel condition (b) Undetectable channel condition

Fig. 3. The dead spot problem of the phase demodulation algorithm.

For simplicity, we assume $x[n] = 1$ in this example so that we can clearly observe the effect of the wireless channels. The colored line denotes the sum of the direct path and the reflected path wireless channels. The amplitude of a received sample may vary according to $x[n]$, but the phase difference is solely affected by the wireless channels as described in Eq. (5). ϕ_0 and ϕ_1 represent the phase difference values for the backscatter bits '0' and '1', respectively. Fig. 3(a) shows the detectable wireless channel condition where $\phi_0 - \phi_1$ is evident so that the phase demodulation algorithm can track the two states. By contrast, ϕ_0 and ϕ_1 cannot describe anything in Fig. 3(b). No matter which bits are transmitted by the tag, the receiver observes the same phase difference values and cannot demodulate any backscatter signal.

As a solution to this problem, we focus on receiver antenna diversity. Because the input of the the phase demodulation algorithm is two received sample sequences from an antenna pair, a receiver with three antennas observes three different wireless channels from $r_1[n]r_2^*[n]$, $r_1[n]r_3^*[n]$, and $r_2[n]r_3^*[n]$, respectively. Similarly, a receiver with four antennas can utilize six different antenna pairs to diversify wireless channel conditions. If there is at least one antenna pair that does not experience the dead spot problem, the receiver can demodulate a backscatter signal from that antenna pair. Fortunately, conventional multiple antenna placement provides enough channel diversity to avoid the dead spot problem. For a 2.4 GHz signal with a wavelength of 12.5 cm, the phase shifts to 90° when the antenna is moved 3.125 cm away from the transmitter's line-of-sight path. Also, the initial phase offsets across receiver radio chains caused by several hardware components improve the diversity of our design, whereas the offsets should be calibrated in device tracking systems [19].

To utilize antenna diversity for backscatter signal detection, we scale out the phase demodulation algorithm. A parallelized backscatter receiver performs the phase demodulation algorithm concurrently for each antenna pair. The receiving procedure succeeds when at least one antenna pair produces a valid backscatter frame that passes the CRC check. If a valid frame is detected, the receiver discards results from the other antenna pairs for the tag symbol duration so as not to return duplicated frames. Additionally, the receiver

Fig. 4. AnyScatter hardware prototype and ambient transmitter devices

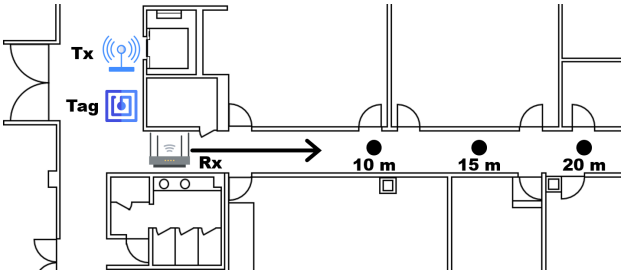

Fig. 5. Experimental setup for AnyScatter performance evaluation

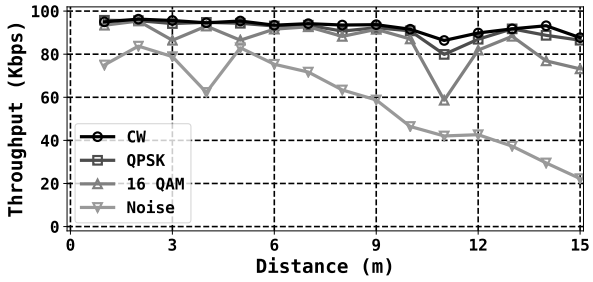

Fig. 6. AnyScatter throughput with four types of carrier sources

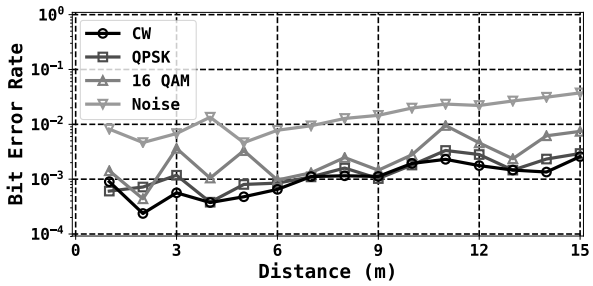

Fig. 7. AnyScatter bit error rate with four types of carrier sources

performs an energy demodulation algorithm for each antenna. The energy demodulation algorithm operates in the same way as the phase demodulation algorithm, except that it compares $|C_0^{'} - \|r_i[n]\|\,|$ and $|C_1^{'} - \|r_i[n]\|\,|$. Although this algorithm can analyze limited types of ambient signals as shown in Fig. 2, the parallel demodulation provides better detection performance for constant envelope ambient signals. To sum up, for example, a parallelized backscatter receiver with four antennas runs six phase demodulation modules and four energy demodulation modules. The pros and cons of this approach are evaluated in the following section.

IV. Performance Evaluation

In this section, we describe how we implement and evaluate AnyScatter on the software-defined radio platform. To show the feasibility of our design, we conduct extensive experiments with various types of ambient sources. We evaluate the backscatter receiver performance while varying the tag-to-receiver distance and the ambient sources. We also evaluate the computational overhead of the receiver in terms of bandwidth and real-time capability.

A. Prototype Implementation

Fig. 4 shows the hardware prototype of our system. We implement an AnyScatter receiver by using two USRP X310s with SBX-120 daughterboards [20]. Both devices share the same reference clocks for device synchronization. A USRP X310 platform supports device-to-device internal clock sharing. Because each device supports up to two receiving antennas, our implementation is based on a receiver with four omni-directional antennas. The USRP X310 converts a received signal to time domain IQ samples and then sends them to a host PC. The host runs the phase and energy demodulation algorithm in parallel. The USRP X310 performs the analog-to-digital conversion for received signals at 200 Msps by default. The samples are decimated to the bandwidth during digital down conversion and then sent to the host, so the sample rate at the host is equal to the bandwidth. In this paper, we set the bandwidth to 50 MHz, the maximum rate that the host can process in real-time. To build an ambient backscatter tag prototype, we use an Artix-7 35T Arty FPGA Evaluation Kit [21] and an HMC284A RF switch [22]. The RF switch has two open circuit transmission lines. Incident signals are reflected at the end of the line. The first line is about 3.125 cm longer than the second line so that the phase difference between two lines becomes $\pi = \lambda/2 = 6.25cm$ at 2.4 GHz. The FPGA board is connected to the RF switch and selects the transmission line to change the reflection coefficient. The tag transmits a 4 bytes frame continuously with 100 Kbps data rate. The receiver compares the results of the demodulators with the transmitted frame to evaluate throughput and bit error rate.

B. Backscatter Throughput and Bit Error Rate

To investigate the effect of ambient sources and communication distance, we conduct experiments in a corridor environment as shown in Fig. 5. The ambient source and the tag are placed at fixed positions with the line-of-sight. The distance from the tag to the receiver varies from 1 m to 20 m along the corridor. The receiver is not in the line-of-sight of the tag in this experiment.

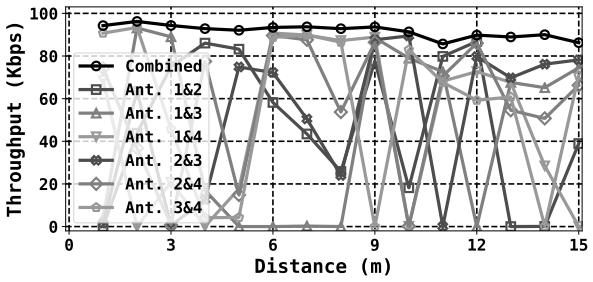

Fig. 8. Phase demodulation throughput over a continuous wave

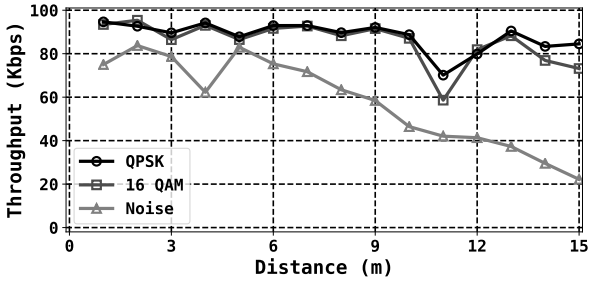

Fig. 10. Phase demodulation throughput over time-varying ambient signals

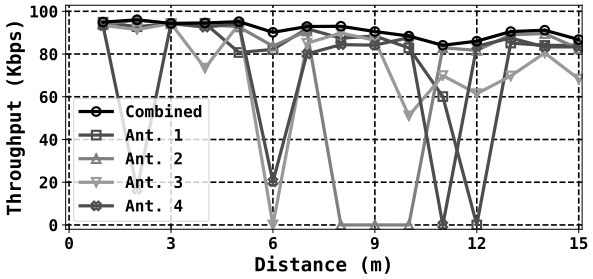

Fig. 9. Energy demodulation throughput over a continuous wave

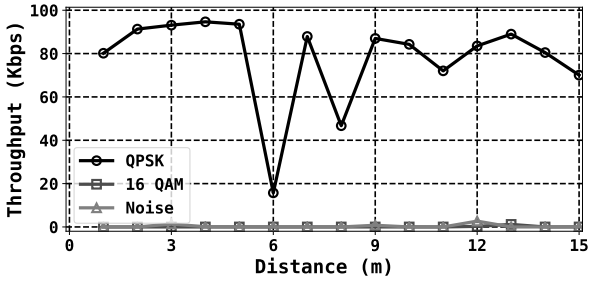

Fig. 11. Energy demodulation throughput over time-varying ambient signals

1) Single-Carrier Backscatter: We use a USRP N210 as an ambient source to generate various types of wireless signals as shown in Fig. 2. The tag is placed 1 m away from the source in this experiment. The receiver covers a frequency range from 2.45 GHz to 2.5 GHz. We set the transmission power of the source to 13 dBm. The center frequency of the source is 2.49 GHz. The source transmits four types of signals, a continuous wave, a QPSK signal, a 16 QAM signal, and a noise signal. The continuous wave is the same as a tone signal of 1 MHz. The bandwidth of the QPSK signal is set to 2 MHz to emulate the IEEE 802.15.4 standard. Random bits are transmitted over the QPSK signal. The same setting is used for the 16 QAM signal. The bandwidth of the noise signal is set to 20 MHz.

Fig. 6 and Fig. 7 shows the throughput and the bit error rate when the receiver moves away from the tag. In the case of a continuous wave, we obtain an 87.6 Kbps throughput at a distance of 15 m. The performance of the continuous wave scenario can be regarded as the upper bound of this evaluation, because it is an ideal carrier signal for backscatter transmission. On the other hand, the results show that the variability of ambient signals has a negative impact on backscatter performance. When the receiver is 15 m away from the tag, we obtain 86.4 Kbps, 73.2 Kbps, and 22.3 Kbps throughput for QPSK, 16 QAM, and noise signals, respectively. The reason for this result can be explained by the approximation in Section III.A. The receiver even decodes backscatter frames from a noise signal as we claimed, because the expected value of the phase difference is coherent unless the tag changes its reflection coefficient. However, we should also consider the variance of the received samples. The variance is regarded as a noise component from the viewpoint of the receiver. The moving average window size of the receiver should be enough long to reduce the variance below the level of backscatter signals. In this regard, we can extend the communication range of the tag by reducing the backscatter data rate, but we fix the data rate of the tag to 100 Kbps to demonstrate ambient backscatter with 2.4 GHz ISM band devices. Note that we can repeat this evaluation for different frequencies and different backscatter data rate without any modifications on our design.

Next, we evaluate how the parallelized receiver with four antennas addresses the dead spot problem. Because the dead spot problem is independent to the ambient signal type, we analyze the backscatter throughput over a continuous wave to observe the dead spots clearly. Fig. 8 shows the throughput of the phase demodulation algorithm for each antenna pair. Even with a strong backscatter signal, the receiver cannot observe anything when the tag is in the dead spot as illustrated in Fig. 3(b). The energy demodulation algorithm suffers from the same problem. Fig. 9 shows the throughput of the algorithm for each antenna. Although the energy demodulation algorithm is less sensitive to the dead spots than the phase demodulation algorithm, it is the same that both algorithms cannot provide stable performance without antenna diversity. This is the reason why we scale out the backscatter receiver. Even though an antenna pair may experience the dead spot problem, one of the other antenna pair can detect a backscatter signal. This gain is also effective to reduce the packet error rate with the same principle. For these reasons, the combined throughput is always better than a single antenna or a single antenna pair throughput results.

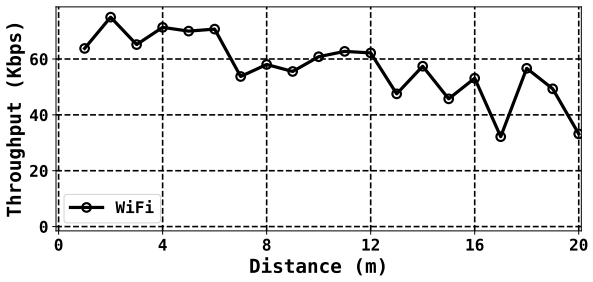

Fig. 12. AnyScatter throughput with a Wi-Fi transmitter

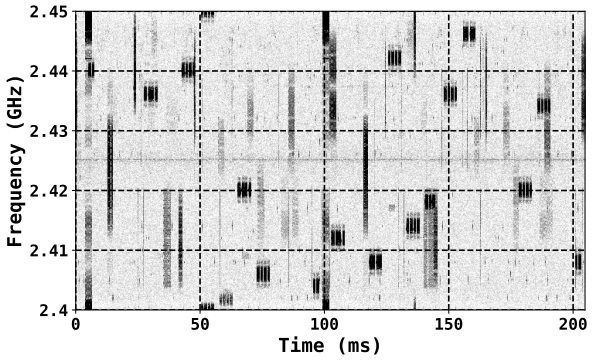

Fig. 13. The spectrogram of Bluetooth traffic

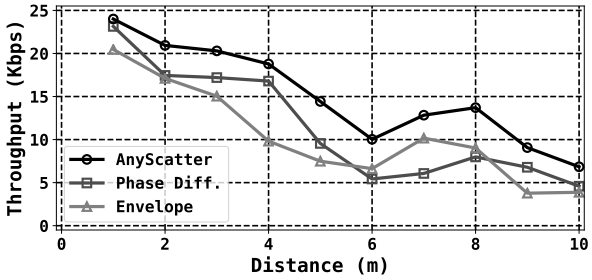

Fig. 14. AnyScatter throughput with a Bluetooth transmitter

We then evaluate whether our approach eliminates technology dependency of ambient backscatter systems. Fig. 10 and Fig. 11 show the throughput of the phase and energy demodulation algorithms for time-varying ambient signals. The phase demodulation algorithm, that we designed in this paper, can analyze every type of ambient signal. By contrast, the energy demodulation algorithm operates only with constant envelope signals, because it cannot extract the effect of a tag from non-constant envelope signals. Apart from technology dependency, the parallelized receiver aggregates both phase and energy demodulation algorithms in the same way as multiple antenna combining. This approach involves additional computational overhead due to increased concurrent modules, but improves backscatter demodulation performance for constant envelope ambient signals. Because the two algorithms have different causes of dead spot problems, the energy demodulation algorithm may decode backscatter frames that are not observed by the phase differences from all pairs of antennas.

2) Wi-Fi Backscatter: To validate the feasibility of our design, we demonstrate ambient backscatter transmission with commodity Wi-Fi devices. We create an 802.11n network on the channel 13 (2472 MHz). A Raspberry Pi connects to a TP-Link Archer C7 access point via a TL-WN722N Wi-Fi USB adapter. We upload the OpenWRT firmware on the access point and run $iperf3$ on both devices to generate UDP traffic from the Raspberry Pi to the access point. The positions of a transmitter, a tag, and a receiver are equal to the previous experimental setup as shown in Fig. 5. The tag of 100 Kbps data rate is deployed 1 m away from the transmitter. The receiver with four antennas covers from 2.45 GHz to 2.5 GHz.

Fig. 12 shows the throughput of Wi-Fi backscatter across tag-to-receiver distances. Our design achieves 60.8 Kbps throughput at 10 m away from the tag and 33.2 Kbps throughput at 20 m away from the tag. This performance is comparable to that of existing Wi-Fi backscatter solutions. It is hard to make an accurate comparison with other solutions because of differences in hardware, but we can say that our prototype provides a similar level of performance to the state-of-the-art ambient backscatter solutions. Also, in contrast to existing solutions, our design has no dependency on carrier signals. Considering that there are various types of wireless devices in terms of wireless technology standards and frequency allocations, our approach is a more promising way to deploy ambient backscatter systems.

3) Bluetooth Backscatter: We also demonstrate ambient backscatter transmission with commodity Bluetooth devices. We use two nRF52840 development kits [23] supporting the Bluetooth 5 standard. The transmission power of the development kit is 0 dBm. We run a default throughput benchmark application between the two development kits. Fig. 13 shows the spectrogram when we run the benchmark application. We can see the 2 MHz bandwidth Bluetooth frames hopping the frequencies. The frequency range of Bluetooth is from 2.4 GHz to 2.485 GHz. However, unfortunately, current implementation supports real-time operation up to 50 MHz bandwidth. We expect that the receiver can analyze 100 MHz bandwidth in real-time after some optimization. For this reason, the receiver with four antennas covers from 2.4 GHz to 2.45 GHz. The tag is placed 50 cm away from the transmitter in this evaluation, because the transmission power is much weaker than other evaluation scenarios.

Fig. 14 shows the throughput of Bluetooth backscatter across tag-to-receiver distances. Similar to the continuous wave and QPSK backscatter scenarios, both phase and energy demodulation algorithms perform roughly the same, whereas the parallelized receiver always shows a better throughput than the two algorithms. Our design achieves 6.8 Kbps throughput at a distance of 10 m. On the other hand, this evaluation validates technology independency of our design in terms of the frequency spectrum. As addressed in [24, 25], because a

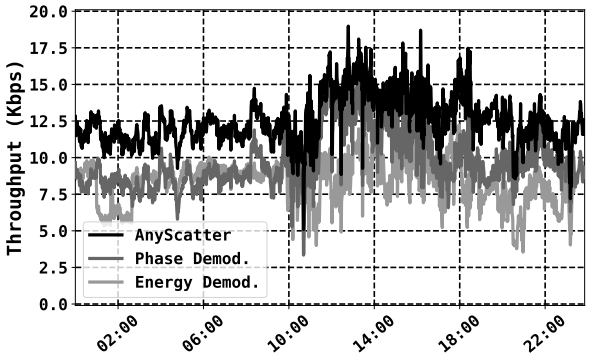

Fig. 15. Ambient backscatter throughput with background traffic

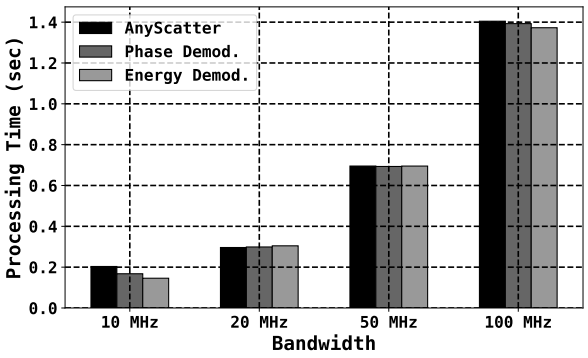

Fig. 16. Processing time for each demodulation algorithm

backscatter tag responds to every incident signal received from an antenna, a backscatter receiver also should be independent of the bandwidth and the center frequency of carrier signals. By demonstrating Bluetooth backscatter, we show that our design meets this demand.

4) Ambient Backscatter: Finally, we investigate how well the tag utilizes background traffic for backscatter transmission. In contrast to the previous experimental setup, we do not deploy an ambient source. We conduct an experiment in our office for a day. A receiver with four antennas is placed 50 cm away from the tag. The frequency range of the receiver is 2.4 GHz to 2.45 GHz. All single stream ambient signals transmitted from user devices in that frequency range are used for backscatter transmission. Fig. 15 shows the result of this evaluation. Our design achieves 12.6 Kbps average throughput. During the daytime from 13:00 to 17:00, the average throughput is increased to 14.4 Kbps.

These results lead to various discussions about our design. The first observation is that more than 10 % of airtime is used for backscatter transmission even at night, since the data rate of the tag is 100 Kbps. We guess that the receiver demodulates backscatter signals from beacon frames in most cases. For example, 802.11b beacon frames can be analyzed with both phase and energy demodulation algorithms. Wi-Fi scan results show that more than 20 access points are present in our office, unlike the corridor environment in Fig. 5 where there are only two access points. Because our design is independent of the carrier frequency, any Wi-Fi beacon can be used as ambient signals, if the signals in the receiver's frequency range. Secondly, the increase in backscatter throughput during the daytime is lower than expected. We expect the tag to take advantage of ambient Wi-Fi frames from user devices such as smartphones. However, most Wi-Fi devices today support MIMO technology. Unless a device selects a single stream mode due to the rate adaptation algorithm, the receiver cannot analyze ambient Wi-Fi frames using spatial stream transmission. Ambient Bluetooth frames are still available for backscatter transmission, but transmission power is too weak in general. Additionally, we should consider the situation where multiple frames are transmitted simultaneously within

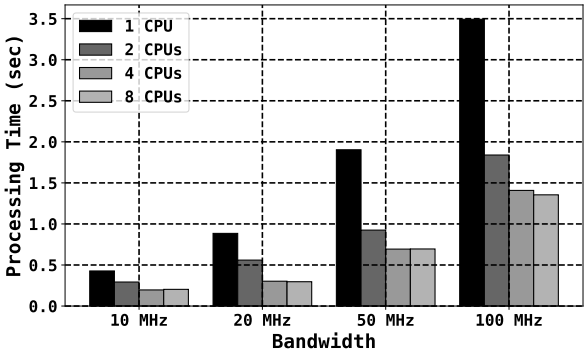

Fig. 17. AnyScatter processing time according to the number of CPUs

the receiver's frequency range. It does not make a problem if one frame is much stronger than others, but otherwise the receiver cannot decode a backscatter frame because transmitted signals are not abstracted to $x[n]$ as in Eq. (3). We may solve this challenge by parallelizing the receiver once again in the frequency domain, but it requires a lot of computational overhead due to parallelization as well as FFT. For this reason, we leave it as future work.

C. Real-time Processing Capability

In this section, we evaluate the processing time of the backscatter demodulation algorithms. As described in Section IV.A, the sample rate is equal to the receiver bandwidth in our implementation. Hence, a receiver should be as simple as possible to analyze wider bandwidth, which guarantees more opportunities to analyze ambient signals. We conduct this experiment on the continuous wave scenario to maximize frame decoding overhead. A receiver with four antennas records received samples from each antenna to a dump file for one second. We measure the processing time for the dump files. If an algorithm takes more than one second to process the dump files, it cannot be implemented in real-time. We run this measurement on a host machine with an Intel Core i7-6700K 4.0 GHz processor, 16 GB DRAM, and a Crucial BX200 480 GB SSD. The GNURadio version that we used is v3.7.13.5.

The processing time increases linearly with the bandwidth as shown in Fig. 16. AnyScatter, the aggregation of phase and energy demodulation algorithms, consumes 0.2, 0.29, 0.69, and 1.4 seconds, respectively, for each bandwidth. By contrast, the type of algorithm has little effect on the processing time. The three algorithms take about 0.7 and 1.4 seconds to process the 50 MHz and 100 MHz bandwidth dump files. This result shows that parallelization incurs negligible overhead compared to other procedures. The VOLK library significantly reduces signal processing overhead, especially for conjugate multiplication and squared magnitude, with SIMD parallelization [26]. We guess that most of the time is spent on input/output data processing. The host machine handles 3.2 GB of received samples per second in the 100 MHz bandwidth setting. Similar overhead occurs when the host machine receives IQ samples from the USRP through the Ethernet interface.

Fig. 17 shows the AnyScatter processing time changed with the bandwidth and the number of CPUs. We use $numactl$ to allocate a fixed number of CPUs to the process. If a host machine does not have sufficient processing power, the real-time bandwidth of a receiver is reduced. When a single CPU is allocated to the process, the energy, phase, and AnyScatter algorithms consume 3.41, 3.62, and 4.29 seconds, respectively, for 100 MHz bandwidth. The parallelization overhead of our design is added up to the processing time when the number of CPUs is less than 4. Our prototype with a commercial host machine with 8 CPUs can provide real-time bandwidth up to 50 MHz and it can be further improved when we reduce the input/output data processing overhead.

V. Related Work

Over the past few years, researchers have found innovative ways to deploy backscatter systems [27]. Traditional backscatter systems are based on the monostatic architecture in which a reader not only transmits a continuous wave but also serves as a backscatter receiver. This architecture enables zero-power communication at passive tags by pushing all the complexity into the reader. However, because the self-interference problem occurs in the reader, only a few meters of read range is provided even with expensive analog components. The bistatic architecture is an alternative way to deploy backscatter systems. By separating a carrier source and a backscatter receiver, this approach drastically increases the read range [28, 29]. Ambient backscatter systems take one step further. Instead of a dedicated carrier source, a tag reflects ambient RF signals and a receiver separates the effect of the tag from the ambient signals. As a result, this approach provides wide backscatter coverage at a low deployment cost compared to traditional backscatter systems.

The first ambient backscatter system demonstrates tag-to-tag backscatter communications by reflecting TV tower signals [4]. And then, multi-antenna and spread spectrum techniques are implemented on the tag for communication performance improvement [5]. The multi-antenna technique is similar to the phase demodulation algorithm in our design, but the two approaches focus on analog hardware implementation and tag-to-tag communications. From the perspective of the tag-to-gateway communication model, several types of ambient backscatter systems have been proposed. Wi-Fi backscatter introduces how to decode backscatter bits with a user device based on the changes in received signal strength [6]. In [8, 30], the changes in error vectors for each Wi-Fi data symbol caused by a tag is exploited for backscatter signal detection. In [25], the authors explain why Wi-Fi frames in different center frequencies also should be analyzed and implement a channel independent Wi-Fi backscatter receiver. Aside from the Wi-Fi standards, there are several attempts to enable backscatter communications over ambient OFDM signals. In [31], the repeating structure of an OFDM signal in the time domain due to the cyclic prefix is used for backscatter signal detection. Similarly, a backscatter modulation scheme exploiting null subcarriers of OFDM signals has been proposed in [32].

Another promising way to design an ambient backscatter system is to shift the frequency of an incident signal. By increasing the clock rate, the tag can utilize frequency-shift keying modulation for backscatter transmission. In recent years, several types of hardware prototypes have been implemented to generate 802.11b [9, 10], single-stream 802.11n [11, 16, 33], and multi-stream 802.11n [34] frames. The same principle has been applied to ambient backscatter designs based on FM radio stations [13, 35] and LoRa gateways [12, 36]. However, these approaches are specialized to a certain type of wireless standard, thus tags and receivers are still dependent on the corresponding infrastructure. It is desirable to eliminate technology dependency from the bottom up rather than mitigating the limitations. The most similar work to our design is the universal backscatter receiver proposed in [37]. The receiver consists of multiple signal processing pipelines specialized to each wireless technology, so technology dependency yet remains in this approach. Nevertheless, the maximum ratio combining technique that the authors developed provides an insight to improve our design.

VI. Conclusion

In this paper, we introduce AnyScatter, a novel design that expands the meaning of the term ”ambient” in backscatter systems. By aligning the received signals from each antenna, AnyScatter enables a backscatter tag to leverage all single-stream wireless devices as carrier sources. We show the feasibility of our approach by demonstrating backscatter transmissions over several types of carrier signals. We further analyze communication performance and technical challenges with extensive experiments. We believe that AnyScatter provides a new paradigm to design ambient backscatter systems without consideration of existing wireless infrastructure.

Acknowledgment

This work was supported by the National Research Foundation of Korea (NRF) grant funded by the Korea government (MSIT) (No. 2019R1A2C2088812). Wonjun Lee is the corresponding author.

REFERENCES

[1] P. Zhang, P. Hu, V. Pasikanti, and D. Ganesan, "Ekhonet: High speed ultra low-power backscatter for next generation sensors," in *Proc. of ACM MobiCom*, 2014.

[2] V. Talla, B. Kellogg, S. Gollakota, and J. R. Smith, "Battery-free cellphone," *Proc. ACM Interact. Mob. Wearable Ubiquitous Technol.*, vol. 1, no. 2, Jun. 2017.

[3] S. Naderiparizi, M. Hessar, V. Talla, S. Gollakota, and J. R. Smith, "Towards battery-free HD video streaming," in *Proc. of USENIX NSDI*, 2018.

[4] V. Liu, A. Parks, V. Talla, S. Gollakota, D. Wetherall, and J. R. Smith, "Ambient backscatter: Wireless communication out of thin air," in *Proc. of ACM SIGCOMM*, 2013.

[5] A. N. Parks, A. Liu, S. Gollakota, and J. R. Smith, "Turbocharging ambient backscatter communication," in *Proc. of ACM SIGCOMM*, 2014.

[6] B. Kellogg, A. Parks, S. Gollakota, J. R. Smith, and D. Wetherall, "Wi-fi backscatter: Internet connectivity for rf-powered devices," in *Proc. of ACM SIGCOMM*, 2014.

[7] D. Bharadia, K. R. Joshi, M. Kotaru, and S. Katti, "BackFi: High throughput WiFi backscatter," in *Proc. of ACM SIGCOMM*, 2015.

[8] T. Kim and W. Lee, "Exploiting residual channel for implicit wi-fi backscatter networks," in *Proc. of IEEE INFOCOM*, 2018.

[9] B. Kellogg, V. Talla, S. Gollakota, and J. R. Smith, "Passive Wi-Fi: Bringing low power to Wi-Fi transmissions," in *Proc. of USENIX NSDI*, 2016.

[10] V. Iyer, V. Talla, B. Kellogg, S. Gollakota, and J. Smith, "Inter-technology backscatter: Towards internet connectivity for implanted devices," in *Proc. of ACM SIGCOMM*, 2016.

[11] P. Zhang, M. Rostami, P. Hu, and D. Ganesan, "Enabling practical backscatter communication for on-body sensors," in *Proc. of ACM SIGCOMM*, 2016.

[12] V. Talla, M. Hessar, B. Kellogg, A. Najafi, J. R. Smith, and S. Gollakota, "Lora backscatter: Enabling the vision of ubiquitous connectivity," *Proc. ACM Interact. Mob. Wearable Ubiquitous Technol.*, vol. 1, no. 3, Sep. 2017.

[13] A. Wang, V. Iyer, V. Talla, J. R. Smith, and S. Gollakota, "FM backscatter: Enabling connected cities and smart fabrics," in *Proc. of USENIX NSDI*, 2017.

[14] P. Hu, P. Zhang, M. Rostami, and D. Ganesan, "Braidio: An integrated active-passive radio for mobile devices with asymmetric energy budgets," in *Proc. of ACM SIGCOMM*, 2016.

[15] Z. Kapetanovic, A. Saffari, R. Chandra, and J. R. Smith, "Glaze: Overlaying occupied spectrum with downlink iot transmissions," *Proc. ACM Interact. Mob. Wearable Ubiquitous Technol.*, vol. 3, no. 4, Dec. 2019.

[16] P. Zhang, C. Josephson, D. Bharadia, and S. Katti, "Freerider: Backscatter communication using commodity radios," in *Proc. of ACM CoNEXT*, 2017.

[17] A. Y. Majid, M. Jansen, G. O. Delgado, K. S. Yildirim, and P. Pawelczak, "Multi-hop backscatter tag-to-tag networks," in *Proc. of IEEE INFOCOM*, 2019.

[18] J. G. Proakis and M. Salehi, *Digital Communications*, 5th ed. McGraw-Hill, 2008, ch. 5.

[19] Y. Xie, J. Xiong, M. Li, and K. Jamieson, "md-track: Leveraging multi-dimensionality in passive indoor wi-fi tracking," in *Proc. of ACM MobiCom*, 2019.

[20] Ettus Research. (2014) SBX Daughterboard RF Performance Data. [Online]. Available: http://files.ettus.com/performance_data/sbx/SBX-without-UHD-corrections.pdf

[21] Digilent. Artix-7 35T Arty FPGA Evaluation Kit. [Online]. Available: https://reference.digilentinc.com/reference/programmable-logic/arty-a7/start

[22] Analog Devices. HMC284A SPDT Non-Reflective Switch. [Online]. Available: https://www.analog.com/media/en/technical-documentation/data-sheets/hmc284a.pdf

[23] Nordic Semiconductor. nRF52840 Development Kit. [Online]. Available: https://www.nordicsemi.com/Software-and-Tools/Development-Kits/nRF52840-DK

[24] Y. Ma, N. Selby, and F. Adib, "Minding the billions: Ultra-wideband localization for deployed rfid tags," in *Proc. of ACM MobiCom*, 2017.

[25] T. Kim and W. Lee, "Channel independent wi-fi backscatter networks," in *Proc. of IEEE INFOCOM*, 2019.

[26] Vector-Optimized Library of Kernels. [Online]. Available: http://libvolk.org/

[27] N. Van Huynh, D. T. Hoang, X. Lu, D. Niyato, P. Wang, and D. I. Kim, "Ambient backscatter communications: A contemporary survey," *IEEE Communications Surveys Tutorials*, vol. 20, no. 4, pp. 2889–2922, Fourthquarter 2018.

[28] J. Kimionis, A. Bletsas, and J. N. Sahalos, "Increased range bistatic scatter radio," *IEEE Transactions on Communications*, vol. 62, no. 3, pp. 1091–1104, Mar. 2014.

[29] P. N. Alevizos, K. Tountas, and A. Bletsas, "Multistatic scatter radio sensor networks for extended coverage," *IEEE Transactions on Wireless Communications*, vol. 17, no. 7, pp. 4522–4535, Jul. 2018.

[30] A. Abedi, M. H. Mazaheri, O. Abari, and T. Brecht, "Witag: Rethinking backscatter communication for wifi networks," in *Proc. of ACM HotNets*, 2018.

[31] G. Yang, Y. C. Liang, R. Zhang, and Y. Pei, "Modulation in the air: Backscatter communication over ambient ofdm carrier," *IEEE Transactions on Communications*, vol. 66, no. 3, pp. 1219–1233, Mar. 2018.

[32] M. A. ElMossallamy, M. Pan, R. Jntti, K. G. Seddik, G. Y. Li, and Z. Han, "Noncoherent backscatter communications over ambient ofdm signals," *IEEE Transactions on Communications*, vol. 67, no. 5, pp. 3597–3611, May 2019.

[33] P. Zhang, D. Bharadia, K. Joshi, and S. Katti, "Hitchhike: Practical backscatter using commodity wifi," in *Proc. of ACM SenSys*, 2016.

[34] J. Zhao, W. Gong, and J. Liu, "Spatial stream backscatter using commodity wifi," in *Proc. of ACM MobiSys*, 2018.

[35] G. Vougioukas and A. Bletsas, "Switching frequency techniques for universal ambient backscatter networking," *IEEE Journal on Selected Areas in Communications*, vol. 37, no. 2, pp. 464–477, Feb. 2019.

[36] Y. Peng, L. Shangguan, Y. Hu, Y. Qian, X. Lin, X. Chen, D. Fang, and K. Jamieson, "Plora: A passive long-range data network from ambient lora transmissions," in *Proc. of ACM SIGCOMM*, 2018.

[37] C. Yang, J. Gummeson, and A. Sample, "Riding the airways: Ultra-wideband ambient backscatter via commercial broadcast systems," in *Proc. of IEEE INFOCOM*, 2017.